

# The geometry of the filamentary environment of galaxy clusters

Yookyung Noh<sup>1</sup> and J.D. Cohn<sup>2</sup>

<sup>1</sup> *Department of Astronomy and Theoretical Astrophysics Center, University of California, Berkeley, CA 94720*

<sup>2</sup> *Space Sciences Laboratory and Theoretical Astrophysics Center, University of California, Berkeley, CA 94720*

30 October 2018

## ABSTRACT

We construct a filament catalogue using an extension of the halo based filament finder of Zhang et al. (2009), in a 250 Mpc/h side N-body simulation, and study the properties of filaments ending upon or surrounding galaxy clusters (within 10 Mpc/h). In this region, the majority of filamentary mass, halo mass, and galaxy richness centered upon the cluster tends to lie in sheets, which are not always coincident. Fixing a sheet width of 3 Mpc/h for definiteness, we find the sheet orientations and (connected) filamentary mass, halo mass and richness fractions relative to the surrounding sphere. Filaments usually have one or more endpoints outside the sheet determined by filament or halo mass or richness, with at least one having a large probability to be aligned with the perpendicular of the plane. Scatter in mock cluster mass measurements, for several observables, is often correlated with the observational direction relative to these local sheets, most often for richness and weak lensing, somewhat less for Compton decrement, and least often for velocity dispersions. The long axis of the cluster also tends to lie in the sheet and its orientation relative to line of sight also correlates with mass scatter.

## 1 INTRODUCTION

Large scale structure in the universe forms a cosmic web (Zel'dovich, Einasto & Shandarin 1982; Shandarin & Zel'dovich 1983; Einasto et al. 1984; Bond, Kofman & Pogosyan 1996), evident in the universe's dark matter, halo, galaxy, and gas distributions. The richness of the cosmic web is evident when one has sufficient statistics and resolution (numerically) or sensitivity (observationally) to see beyond the densest structures, correspondingly there has been a wealth of study of its properties. Examples include characterization of average properties (e.g. see Schmazling (1998) for one early review, Shandarin (2004); van de Weygaert et al. (2010); Shandarin (2010) for some more recent papers and references within), identifying the web in observations and simulations (e.g., Bharadway et al. (2000); Pimblet, Drinkwater & Hawkrigg (2004); Feix et al. (2008); Sousbie et al. (2008a); Bond, Strauss & Cen (2009); Way, Gazis & Scargle (2010); Bond, Strauss & Cen (2010); Choi et al. (2010); Mead, King & McCarthy (2010); Murphy, Eke & Frenk (2010); Sousbie, Pichon & Kawahara (2010), tracing its relation to initial conditions (e.g., Shandarin, Habib & Heitmann (2009)) and comparing filamentary environments and properties of galaxies within them (spin, shapes, alignments and more: Lee (2004); Lee et al. (2008); Altay, Colberg & Croft (2006); Aragón-Calvo et al. (2007b); Dolag et al. (2006); Pandey & Somnath (2006); Faltenbacher et al. (2007); Ragone-Figueroa & Plionis

(2007); Hahn et al. (2007a,b); Paz, Stasyszyn & Padilla (2008); Betancort-Rijo & Trujillo (2009); Gay et al. (2009); Schaefer (2009); Zhang et al. (2009); Hahn, Teyssier & Carollo (2010); Jones, van de Weygaert & Aragón-Calvo (2010); Wang et al. (2010)). Cluster alignments and formation, presumably or explicitly along filaments, have also been studied, e.g. van de Weygaert & Bertschinger (1996); Splinter et al. (1997); Colberg et al. (1999); Chambers, Melott & Miller (2000); Onuora & Thomas (2000); Faltenbacher et al. (2002); van de Weygaert (2002); Hopkins, Bahcall & Bode (2004); Bailin & Steinmetz (2005); Faltenbacher et al. (2005); Kasun & Evrard (2005); Lee & Evrard (2007); Lee et al. (2008); Pereira, Bryan & Gill (2008); Costa-Duarte, Sodre, & Durret (2010), and several observed systems with filaments have been analyzed in detail, some examples are found in Porter & Raychaudhury (2005); Gal et al. (2008); Kartaltepe et al. (2008); Tanaka et al. (2009). Numerous methods for identifying filaments, suitable for different applications, have been proposed (for example Barrow, Bhavsar & Sonoda (1985); Mecke, Buchert & Wagner (1994); Sahni, Sathyaprakash & Shandarin (1998); Schmazling et al. (1999); Colombi, Pogoyan & Souradeep (2000); Sheth et al. (2003); Pimblet (2005a,b); Stoica et al. (2005); Novikov, Colombi & Dore (2006); Aragón-Calvo et al. (2007a); Colberg (2007); van de Weygaert & Schaap (2007); Sousbie et al. (2008b); Stoica, Martinez & Saar (2008); Forero-Romero et al.

(2009); Gonzalez & Padilla (2009); Pogosyan et al. (2009); Sousbie, Colombi & Pichon (2009); Stoica, Martinez & Saar (2009); Wu, Batuski, & Khalil (2009); Genovese et al. (2010); Murphy, Eke & Frenk (2010); Shandarin (2010); Sousbie (2010); Way, Gazis & Scargle (2010)), see Zhang et al. (2009); Aragón-Calvo, van de Weygaert & Jones (2010) for some comparisons of these. Analytic studies of filaments include estimates of their multiplicity (Lee 2006; Shen et al. 2006), anisotropy (e.g. Lee & Springel (2009)), the merger rates of halos into them (Song & Lee 2010) and properties in non-Gaussian theories (De Simone, Maggiore, & Riotto 2010).

Galaxy clusters (dark matter halos with mass  $M \geq 10^{14} h^{-1} M_{\odot}$ ) are of great interest for many reasons, in part because of their sensitivity to cosmological parameters, but also as hosts of the most massive galaxies in the universe, as environments for galaxy evolution more generally, and as the largest virialized objects in the universe with correspondingly special astrophysical processes and histories (for a review see e.g. Voit (2005)). Galaxy clusters tend to lie at nodes of the cosmic web, with matter streaming into them from filaments (e.g. van Haarlem & van de Weygaert (1993); Diaferio & Geller (1997); Colberg et al. (1999)). Although the universe is isotropic and homogeneous on large scales, around any individual cluster there will be directionally dependent density fluctuations due to the condensation of filamentary and sheetlike matter around it. Our interest here is in characterizing this nearby (within 10 Mpc/h) filamentary environment of galaxy clusters. This environment feeds galaxy clusters and is also unavoidably included for many observations of the cluster at its center. This correlated environment is one source of the observationally well known “projection effects,” which have plagued optical cluster finding starting with Abell (1958) and later (e.g. Dalton et al (1992); Lumsden et al (1992); van Haarlem et al. (1997); White et al (1999)), cluster weak lensing, e.g., (Reblinsky & Bartelmann 1999; Metzler, White & Loken 2001; Hoekstra 2001; de Putter & White 2005; Meneghetti et al. 2010; Becker & Kravtsov 2010), cluster Sunyaev-Zel’dovich (Sunyaev & Zel’dovich 1972, 1980) (SZ) flux measurements, e.g., (White, Hernquist & Springel 2002; Holder, McCarthy & Babul 2007; Hallman et al 2007; Shaw, Holder & Bode 2008) and cluster velocity dispersions, e.g., (Cen 1997; Tormen 1997; Kasun & Evrard 2005; Biviano et al. 2006). The environments of clusters have been studied within several contexts and using several methods, e.g. galaxy and dark matter density around clusters (Wang et al. 2009; Poggianti et al. 2010), filamentary growth (e.g. van de Weygaert (2006)) around clusters, filamentary counts (Colberg, Krughoff & Connolly 2005; Aragón-Calvo, van de Weygaert & Jones 2010; Aragón-Calvo, Shandarin & Szalay 2010), in particular the geometry and properties of superclusters, e.g., Shadarin, Sheth & Sahni (2004); Basilakos et al (2006); Wray et al. (2006); Costa-Duarte, Sodre, & Durret (2010), and the cluster alignment studies such as mentioned above.

Here we describe our findings on local cluster environments obtained by implementing the halo-based filament finder of Zhang et al. (2009) in a high resolution N-body simulation. After refining the finder slightly

for our purposes, we obtain a filament catalogue, and consider those filaments connected to or in the vicinity of galaxy clusters. Our work is most closely related to that of Colberg, Krughoff & Connolly (2005); Aragón-Calvo, van de Weygaert & Jones (2010). They used simulations to measure counts of filaments (found via different algorithms) ending upon clusters and average filamentary profiles and curvature. We go beyond these to measure the statistics of the local geometry of filaments around their cluster endpoints. Related studies of filament geometry, particularly for superclusters are found in e.g., Aragón-Calvo, van de Weygaert & Jones (2010); Aragón-Calvo, Shandarin & Szalay (2010), the former also discuss the tendency of filaments around voids and clusters to lie in sheets. We find that most of the filamentary (and halo) material in a 10 Mpc/h sphere around clusters lies in a plane, presumably the one from which the filaments collapsed, and investigate different ways of defining such a plane’s orientation. Many measures of cluster masses include the cluster environment and as a result scatter the mass from its true value. In mock observations on simulations, we find that line of sight dependent scatter in measured cluster masses, for several methods, is often correlated with the angle between the line of sight and these locally defined planes.

In §2 we describe the simulations, mock observations, and filament finder. In §3 we describe the statistical properties of the filaments and matter distribution around clusters, in §4 we consider the geometry of the filament, mass and richness distributions within 10 Mpc/h of each cluster, focussing particularly on planes maximizing these quantities, in §5 we compare scatter in cluster masses to orientation of observations with these planes, and in §6 we conclude.

## 2 SIMULATIONS AND METHODS

### 2.1 Simulation

We use a dark matter only simulation, in a periodic box of side 250 Mpc/h with  $2048^3$  particles evolved using the TREEPM (White 2002) code, and provided to us by Martin White. It is the same simulation as used in White, Cohn & Smit (2010) (hereafter WCS), which can be consulted for details beyond those found below. The background cosmological parameters are  $h = 0.7$ ,  $n = 0.95$ ,  $\Omega_m = 0.274$ , and  $\sigma_8 = 0.8$ , in accord with a large number of cosmological observations. The simulation has outputs at 45 times equally spaced in  $\ln(a)$  from  $z = 10$  to 0. We focussed on  $z = 0.1$ , in part to allow comparison with observational quantities in §5. Halos are found using a Friends of Friends (FoF) halo finder (Davis et al. 1985), with linking length  $b = 0.168$  times the mean interparticle spacing. Masses quoted below are FoF masses.

Resolved subhalos in this high resolution simulation are of importance for the observational comparisons in §5, and for measurements of galaxy properties around and in the clusters. Subhalos are found via FoF6d (Diemand, Kuhlen & Madau 2006), with the specific implementation as described in the appendix of WCS. The subhalos correspond to galaxies with luminosities  $\geq 0.2L^*$  at

$z = 0.1$ <sup>1</sup>, and match observations as described in WCS. The halo and subhalo catalogues and dark matter particles can be combined to produce mock observations for six cluster mass measures. These are (see WCS for specifics and tests of the catalogue): two richnesses (one using the MaxBCG (Koester et al. 2007) algorithm based upon colors<sup>2</sup>, and one based upon spectroscopy (Yang, Mo & van den Bosch 2008)), SZ flux or Compton decrement (flux within an annulus of radius  $r_{180b}$ , the radius within which the average mass is greater than or equal to 180 times background density), weak lensing (using an SIS or NFW model to assume a cluster lens profile and then fitting for a velocity dispersion and then mass), and two velocity dispersions (one based on a simple  $3-\sigma$  clipping, the other on a more complex method using phase space information to reject outliers and calculating mass using a measured harmonic radius as well, based on methods of den Hartog & Katgert (1996); Biviano et al. (2006); Wojtak et al. (2007)); more detail is in WCS. We will use the mass measurements by WCS via these methods, taking cylinders of radius  $r_{180b}$  when a radius choice is required. Just as in that work, lines of sight for clusters are removed a more massive cluster has its center within this radius along the observational line of sight.

## 2.2 Filament finder

We find filaments using an extension of the method described in Zhang et al. (2009). They identify filaments as bridges in dark matter halos above a threshold halo mass overdensity, of length up to 10 Mpc/h. It is analogous to the spherical overdensity finder for clusters, where the cluster radius is taken to be that where the average density around the central point drops below some threshold; here the filament radius is where the average density along the cylinder axis drops below some threshold. Just as there are many different halo finders, there is no unique filament finder or definition. This finder is but one of many different ones present in the literature, which are not only based upon such bridge-like definitions, but also include finders constructed around filtering procedures, potential or density gradients, dynamical information, and more (see Zhang et al. (2009) for some comparisons between their finder and others). Even for a given filament finder, catalogues often must be specified by the finder parameters as well (e.g. smoothing length for density or potential based finders, unbinding criteria for dynamically based finders, etc.). We use the parameters as given in Zhang et al. (2009).

The algorithm of Zhang et al. (2009) is as follows: halos are ordered most to least massive. All halos with mass  $\geq 3 \times 10^{10} h^{-1} M_{\odot}$  are included<sup>3</sup>, mass in the following only refers to that in halos with this mass or above. Starting with the most massive halo (“node”), all halos within 10 Mpc/h but at least 3 Mpc/h away in radius (or  $r_{200c}$ , if greater) are considered as potential endpoints. For each potential endpoint, the cylinder radius is varied, up to 3 Mpc/h, to get the

highest overdensity of halo matter in the cylinder between the node and potential endpoint. This maximum density is then compared to a minimum overdensity (5 times background matter density in halos), and if over this minimum, this endpoint and its radius are kept. If no potential endpoints have a halo mass density for their filament greater than the minimum overdensity then the algorithm moves to the next node. Once all such maximal filaments are found for a given node, the filament with the largest density is kept. The filament is then truncated: its new endpoint is the most massive halo within it which has at least 3 other halos between in and the central node, and which is at least 3 Mpc/h away from the central node. All filament members are then removed from the list of potential future filament members or endpoints around any node. The endpoints are not removed from the list of possible endpoints for other nodes, but are removed from the list of possible endpoints associated with this node. This procedure is repeated until no more new filaments are found around the node.

As this procedure frequently produces many more filaments than were evident by eye around clusters (sometimes over thirty around a single cluster), we incorporate a growing and merging procedure as well. After finding the filaments of maximum density around a given node, we grow out the filament radii until the average mass density in halos within the cylinder stretching to the filament endpoint drops to less than the minimum overdensity, or the maximum 3 Mpc/h radius is reached. Halos lying in two or more such extended filaments are assigned to the one whose axis is closest. Filament endpoints with length  $\ell$  and a perpendicular distance  $d_{\perp}$  to another (longer) filament’s axis such that  $d_{\perp}/\ell < 3/10$  (the maximum width/maximum length in the algorithm) are merged into the longer filament, unless the shorter filament’s endpoint has other filaments extending out of it. (This allows filament radii  $> 3$  Mpc/h.) These new filaments are then given a central axis determined by the center of mass of the filament; filaments whose endpoints do not have additional filaments extending out of them and whose endpoints are within 25 degrees of each other are merged. This is done in order of closest to most distant pairs; if  $> 2$  filaments are within this range, the two closest are merged, then centers of mass are recalculated to see if the remaining filaments are within the minimum distance, and so on.

The resulting filaments are regions connecting halos with halo mass overdensity at least 5 times the background halo mass density, and which are less than 10 Mpc/h long. The full catalogue at  $z = 0.1$  has  $\sim 30,000$  filaments and  $\sim 44,000$  endpoints, with 45% of the halo mass fraction in filaments and 36% of the halos (in number fraction) in filaments. 60% of the  $\sim 1.2 \times 10^6$  halos above the minimum mass cut are not either endpoints or in filaments, with the most massive of these having  $M = 2.6 \times 10^{12} h^{-1} M_{\odot}$ .<sup>4</sup>

Several of the other finders produce filaments which can extend well beyond our 10 Mpc/h cutoff (e.g. Colberg, Krughoff & Connolly (2005) found filaments out

<sup>1</sup> Approximately -18.5 in  $r$  band, see WCS for more discussion.

<sup>2</sup> Color assignments are estimated using the prescription of Skibba & Sheth (2009) with evolution of Conroy, Gunn & White (2009); Conroy, White, & Gunn (2010); Conroy, & Gunn (2010).

<sup>3</sup> This is the minimum mass used by Zhang et al. (2009) converted (see White (2001)) to our FoF definition.

<sup>4</sup> Analytic estimates of filamentary mass fractions mentioned above (which use other filament definitions) are not directly comparable because the latter are based upon total mass; mass in halos above our minimum is only 40% of the mass in the box at  $z = 0.1$ .

to 50 Mpc/h, even longer ones have been found by e.g. Gonzalez & Padilla (2009)), some have restrictions on filament nodes (e.g. Colberg, Krughoff & Connolly (2005) filaments end only on clusters). Our catalogue has straight filament segments  $\leq 10$  Mpc/h in length, built out of dark matter halos above some minimum overdensity which emanate from clusters and other endpoints. Longer filaments could presumably be constructed as chains of our shorter ones, augmented by a condition on how much a filament can bend before it is considered instead to be two separate filaments meeting at a node. The length restriction of our finder also affects breakdowns into mass fraction in filaments, nodes, and so on, as some of our nodes will instead be filament members if the filaments are extended this way.

The work most similar to ours in focus, studying clusters as filament endpoints, is in Colberg, Krughoff & Connolly (2005), some related results are also found and compared in Aragón-Calvo, van de Weygaert & Jones (2010) (see also Sousbie, Pichon & Kawahara (2010), who found a cluster as an intersection of filaments in observational data). Colberg, Krughoff & Connolly (2005) found filaments by looking for matter overdensities by eye between cluster endpoints and measured a wide range of filament statistics, including the number of filaments per cluster as a function of mass, stacked filament profiles, length distributions, and the fractions of cluster pairs connected by filaments. Aragón-Calvo, van de Weygaert & Jones (2010) found filaments using a Multiscale Morphology Filter (see their paper for details) and considered similar quantities to Colberg, Krughoff & Connolly (2005), and in addition introduced a classification for filaments.

### 3 STATISTICS OF FILAMENTS AROUND CLUSTERS

Our finder is well suited to characterize the local environment of clusters, our target of study here. Of the 242 clusters ( $M \geq 10^{14} h^{-1} M_{\odot}$ ) in our box, 226 are also nodes, with  $\sim 1700$  filaments. We restrict to these clusters below. The other 7% (16) of the clusters are within filaments linking two more massive clusters, in addition, 29 of the clusters have a cluster within a filament, and 41 cluster pairs are within a 10 Mpc/h radius of each other. We use the term “connected” filamentary mass to refer to halo mass within a filament connected directly to a cluster, up to and including its other endpoint.<sup>5</sup> In addition to connected filaments around a cluster, within the 10 Mpc/h sphere we will also

<sup>5</sup> The finder, even with modifications, still produced some configurations which we modified with post-processing. For example, sometimes a filament would be found with a large “gap” in the center, where the gap is due to a previously found filament between two other clusters which crosses the region. Even with this gap, the new filament is above our overdensity threshold. As the previous and new filaments seem joined and perhaps one object, we added all the mass (within 10 Mpc/h) of any previously found filament which came within 3Mpc/h to the connected filamentary mass of the cluster, this happened for  $< 10$  of our  $\sim 7000$  filaments.

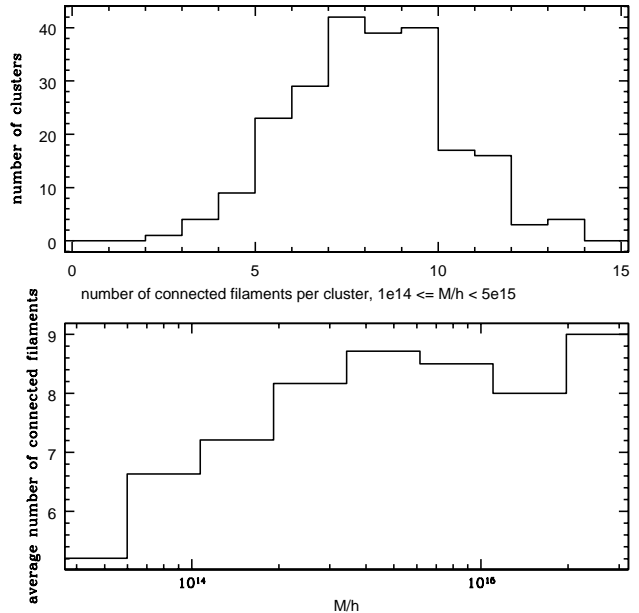


**Figure 1.** Top: distribution of number of filaments per cluster (halos with  $M \geq 10^{14} h^{-1} M_{\odot}$ ). Bottom: number of filaments as a function of mass for all halos which are filament endpoints.

consider all filaments and their endpoints, all halos above our minimum mass of  $3 \times 10^{10} h^{-1} M_{\odot}$ , and all galaxies.

In the 10 Mpc/h spheres surrounding clusters, connected filaments constitute  $\sim 70\%$  of the halo mass on average, but with a very broad distribution of values for individual clusters. A line passing through the 10 Mpc/h shell centered on a cluster will hit one of the original connected filament cores (from the first step of our algorithm) about 10% of the time on average, and one of the grown and merged filaments closer to  $\sim 30\%$  of the time, with a wide spread as well. All (not only connected) filaments in this sphere contain closer to  $\sim 90\%$  of the halo mass, with much less cluster to cluster scatter. (These additional filaments connect two other halos, which may or may not lie within the sphere themselves, rather the cluster and another halo.) In 10 Mpc/h spheres around 10,000 random points, in comparison, the filaments have a halo mass fraction ranging from 60% to 95%.

The distribution of number of connected filaments around clusters, with our finder, is shown at the top of Fig. 1, clusters tend to have 7-9 filaments. We find more massive halos have more filaments ending upon them, shown in Fig. 1, bottom, just as found by Colberg, Krughoff & Connolly (2005); Aragón-Calvo, van de Weygaert & Jones (2010) with their different finders. In addition, connected filaments around clusters tend to be shorter than their counterparts for the much less massive nodes.

The large number of filaments found by the algorithm can be compared to a simplified picture where nodes are fed by a small number of filaments (e.g. 3 or fewer, Keres et al. (2005, 2009); Dekel et al. (2009)). The mass fraction in the largest 2 or 3 filaments is substantial, leading to a partial

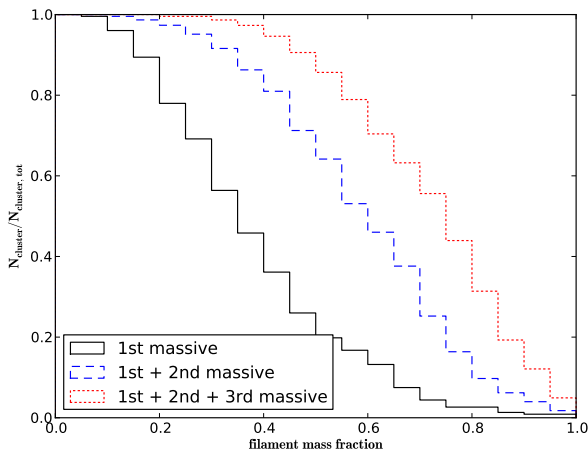


**Figure 2.** Cumulative fraction of filamentary mass in 1 (solid line), 2 (dashed line) and 3 (dotted line) most massive cluster filaments, as fraction of the number of clusters. For example, about half of the clusters have at least 60% of their connected filament mass in their two largest filaments and at least  $\sim 75\%$  of their mass in their three largest filaments.

reconciliation of these pictures, as seen in Fig. 2, that is about half of the clusters have at least  $\sim 75\%$  of their mass in their three largest filaments.

More massive halos have more filaments around them, more matter in filaments, and more matter around them generally, and although the number of filaments for clusters can be quite large, a significant fraction of the filamentary mass is found within the three largest filaments.

#### 4 PLANAR GEOMETRY AROUND CLUSTERS

Filaments provide an anisotropic environment for galaxy clusters. Some approximate trends in the filamentary distribution are accessible via the inertia tensor of its mass, even though filaments are not expected to fill out an ellipsoid. For our clusters, the moment of inertia tensors tend to have two relatively large eigenvalues and one smaller one (corresponding to axis ratios  $a > b \sim c$ , the classic prolate cluster shape, there are many studies of cluster ellipticities, see e.g. Jing & Suto (2002).) In comparison, for connected filaments attached to our clusters, the middle eigenvalue of the inertia tensor tends to be smaller so that the filament distribution is “flatter” than the cluster it surrounds.<sup>6</sup> The long axis of the cluster has a tendency to lie within the “flat” directions of the filamentary distribution, and the eigenvector of the cluster’s inertia tensor that is perpendicular to the long and middle axes of the cluster (i.e.

<sup>6</sup> The connected filament distribution becomes more and more cylindrical with decreasing (well below  $10^{14} h^{-1} M_{\odot}$ ) central halo mass, with the two largest eigenvalues tending to become equal, and the third becoming smaller and smaller. One reason is that lower mass halos are expected to be within filaments, rather than to serve as endpoints; the algorithm used here will tend to break these longer filaments up into more segments as mentioned earlier.

corresponding to the largest eigenvalue) tends to align with the corresponding direction of the filamentary inertia tensor. (See also van de Weygaert (2006); Hahn et al. (2007b); Aragón-Calvo et al. (2007b); Paz, Stasyszyn & Padilla (2008); Aragón-Calvo, van de Weygaert & Jones (2010); as our nodes will sometimes be members of filaments in other finders, some of these alignments are relevant filament member alignment discussed therein.)

Visual inspection of many of our clusters suggests that the majority of their filamentary mass lies within sheetline regions, presumably those from which they condensed (see for example some cases illustrated in Aragón-Calvo, Shandarin & Szalay (2010), and discussion of different filament types in Aragón-Calvo, van de Weygaert & Jones (2010) and their “grid” and “star” configurations).

To quantify this planarity, we consider four definitions of planes, regions extending  $\pm 1.5$  Mpc/h above and below the central cluster and out to the edge of the local 10 Mpc/h sphere. We choose their orientations (normals) so the planes contain the maximum of either 1) connected filament mass, with extra constraints described below, 2) all filamentary mass including endpoints, 3) total halo mass, or 4) number of galaxies, within the 10 Mpc/h sphere. The connected filament mass plane has its normal chosen to be perpendicular to the axes constructed out of a pair filament endpoints; this definition has stronger correlations with observables (discussed later) than using pairs of connected filaments without their endpoints, or using the plane maximizing connected filament mass with no other constraints. The mass in the plane (or richness, when using galaxies) does not include that of the central cluster, as our interest is in the cluster’s environment. In Fig. 3 the objects used for these four choices of plane are shown for a cluster of mass  $2.7 \times 10^{14} M_{\odot}/h$ . It has about 84% of its mass in the connected filament plane.

These four planes tend to have similar orientations, with the all filament and halo mass planes are most often aligned (over 96% clusters have these two normals within 30 degrees). This is not surprising given the dominance of filamentary mass in the 10 Mpc/h sphere around the cluster noted earlier. For a given cluster, the largest misalignment between any pairs of planes tends to be between its connected filament plane and one of the other planes, which for 15% of the clusters differs by another plane by more than 60 degrees. For most clusters it thus seems that the connected filaments are not as closely aligned with the other planes, which extend further out into the sphere. Plane pairs besides the closely aligned all filament and halo mass plane have on average 5–10% of the clusters mismatching by  $>60$  degrees.

The mass or richness fractions in these planes is significantly higher than the fraction ( $\sim 1/5$ ) of volume which the plane occupies in the sphere. The distribution of connected and total filament mass fractions, in the corresponding planes, for our clusters is shown at top in Fig. 4, at bottom is the distribution for the total halo mass plane. Also shown at bottom is the mass fraction for halo mass planes constructed around 10,000 random points (rescaled to have the same area under the curve), which is smaller on average than around the clusters. The richness fraction, not shown, peaks slightly more sharply than the halo mass fraction, but at a lower fraction ( $\sim 60\%$ ). For all plane definitions, 80% of the clusters have more than 60% of their mass (or 55% of

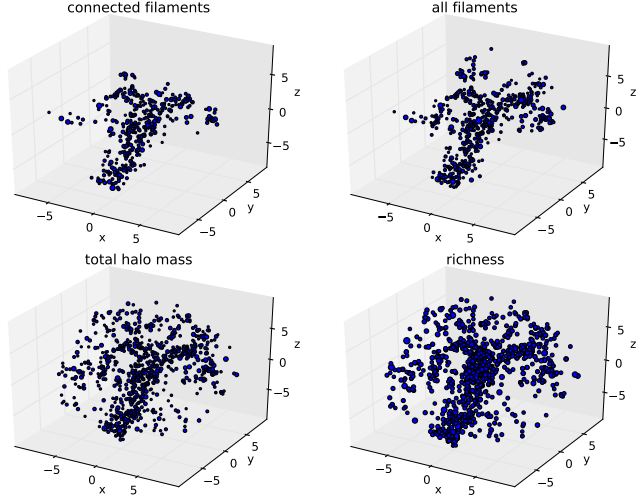


**Figure 3.** Four types of objects used in constructing planes in a 10 Mpc/h radius sphere centered on a  $2.7 \times 10^{14} h^{-1} M_{\odot}$  cluster. Left to right, top to bottom are halos in connected filaments, halos in all filaments, all halos above  $3 \times 10^{10} h^{-1} M_{\odot}$  mass cut, and galaxies above  $0.2L^*$  cut (galaxies in cluster are not shown). Point size is proportional to halo mass or, for richness, halo infall mass (which determines luminosity, see WCS). About 84% of the cluster’s connected filament mass is in the connected filament plane.

their richness) in these planes; about a quarter of the clusters fell below this fraction for at least one plane definition. Our choice of plane height,  $\pm 1.5$  Mpc/h to give 3 Mpc/h in total, was motivated by the characteristic scale of cluster radii. We explored mass plane heights from 1-3 Mpc/h (total plane widths 2-6 Mpc/h), and found that the total halo mass fraction scaled as  $M_{\text{plane}}/M_{\text{sphere}} \sim \text{height}^{1/4}$ . It would be interesting to understand this scaling in terms of intrinsic filament profiles.

The clusters with large plane misalignments (by  $> 60$  degrees) have low mass or richness fractions, or larger mass within 3 Mpc/h of the normal of the connected filament plane (but outside of it) almost twice as often as in the full sample (i.e. in  $\sim 2/3$  of the clusters with mismatched planes). The misaligned plane clusters have only slightly more often a recent<sup>7</sup> merger or a larger intrinsic cluster flatness (as measured by its inertia tensor), they were equally likely to have other clusters within 10 Mpc/h as in the full sample.

The connected filament plane’s normal, similar to its counterpart for the connected filament’s inertia tensor, tends to be aligned with its counterpart for the cluster’s mass inertia tensor, and the cluster’s long axis is likely to lie in the filament plane. The cluster galaxy positions, have an inertia tensor (setting mass to one) which appears uncorrelated with this plane, but restricting to more luminous ( $> 0.4L_*$ , see WCS for detail) galaxies gives an inertia tensor whose “most flat” (perpendicular to eigenvector for largest eigenvalue) direction prefers alignment with the normal to the connected filamentary plane, and whose “long” axis tends to

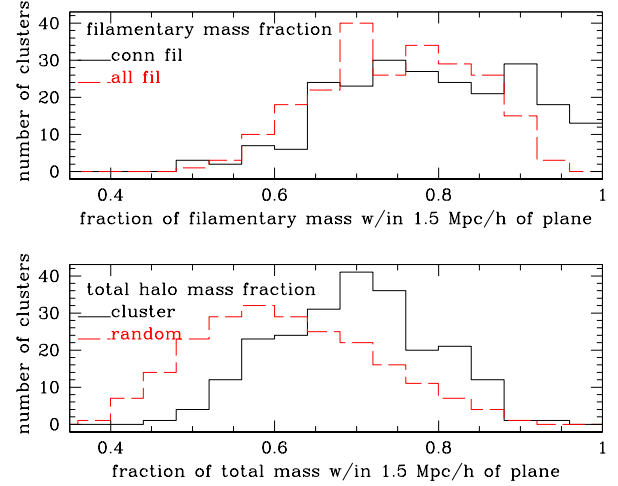


**Figure 4.** Top: Fraction of connected filament mass in connected filament plane (solid) and fraction of all filamentary mass within all filament plane (dashed), both in the fiducial 10 Mpc/h sphere around clusters. The normals to these planes are within 30 degrees for  $\sim 80\%$  of the clusters. Bottom: The fraction of total halo mass (above our  $3 \times 10^{10} M_{\odot}/h$  cutoff) in the mass plane around clusters (solid), and its counterpart around 10,000 random points (dashed), rescaled to have the same number volume as cluster histograms. A large fraction of the filamentary mass and total halo mass in 10 Mpc/h spheres around clusters resides within this planar region containing  $\sim 20\%$  of the volume.

be within the filament plane. The galaxy velocity dispersions are larger along the connected filament plane than perpendicular to it, but are more correlated (e.g. Kasun & Evrard (2005); White, Cohn & Smit (2010)) with the inertia tensor of the cluster itself.

Not all filaments lie in these planes. Filamentary mass can extend outside of the plane, as mentioned earlier, as can filament endpoints. The fraction of filament endpoints lying outside the connected filament plane is shown in Fig. 5, note that this does not preclude a significant amount of the filament’s mass lying within the plane. There is also an increased likelihood for at least one endpoint to lie perpendicular to the connected plane, as shown in Fig. 5 bottom. The distributions in Fig. 5 are similar for the other plane choices. About 1/10 of the clusters have more than  $\sim 3\%$  of their connected filamentary mass within a 3 Mpc/h radius of the normal to their plane but above or below the plane itself, which we refer to as perpendicular filaments below. In addition 10 clusters have over 15% of their mass in a region within 6 Mpc/h radius of the normal, but outside the connected plane.

As noted earlier (Fig. 2), the two most massive connected filaments often do possess a large fraction of the connected filament mass. The plane defined by these two filaments coincides with the connected filamentary mass plane almost half of the time.<sup>8</sup> For 1/3 of the clusters, however, less than half of the connected filament planar mass comes from these two most massive segments. So although the two

<sup>7</sup> Specifically, a satellite which has fallen into the cluster within the last time step,  $\sim 600 \text{ Myrs}$ , which had at the earlier time at least 1/10 of the cluster’s final mass at  $z = 0.1$ .

<sup>8</sup> We thank G. Jungman for asking us to measure this.

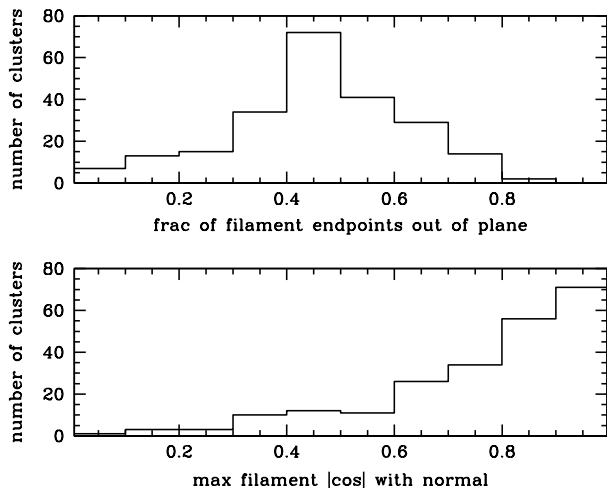


**Figure 5.** Top: fraction of filament endpoints lying outside of connected filament plane- many filaments do not have their endpoints in this plane, even though a large fraction of mass is in this plane (see Fig. 4). Bottom: angle to normal of connected mass plane, for filament closest to the normal; at least one filament tends to be perpendicular to this plane. The corresponding distributions for other planes are similar.

most massive segments have a preponderance of filamentary mass (Fig. 2), their large mass is not wholly responsible for the dominance of planar structure.

The persistence of the locally defined planes to larger radii can be studied by fixing the plane height and orientation, and extending the plane out into a region of 20 Mpc/h in radius, and calculating the fractional mass in this larger plane within the larger sphere. The plane volume fraction of the sphere volume drops by about one half compared to its value in the 10 Mpc/h sphere, but the (all) filamentary mass, halo mass and richness fractions in their respective planes drop by even more, by a factor of  $\sim 40\%$ . There are filamentary, mass or richness planes in this larger sphere of the same  $\pm 1.5$  Mpc/h width which have more of the filamentary, mass or richness in them (and usually more than  $1/2$  the mass fraction of those defined within 10 Mpc/h). These 20 Mpc/h filament and mass planes differ from their counterparts at 10 Mpc/h by over 30 (60) degrees one half (one quarter) of the time, with slightly smaller fractions for the corresponding richness plane.

We did not find a more useful measure of isotropy in the plane (i.e. in the angular direction), although the moment of inertia tensor can indicate how much the planar geometry tends to cylindrical (related questions have been explored when classifying filaments, e.g. (Aragón-Calvo, van de Weygaert & Jones 2010) note a “star” geometry for sets of filaments). One possible consequence of isotropy, or its lack, in the plane will be discussed in the next section on mass measurements.

In summary, as has been known, the mass around clusters tends to lie in filaments, which themselves tend to lie within sheets. We have taken a set sheet width centered on the cluster and maximized different quantities (filament mass, connected filament mass, total halo mass and galaxy

richness) within a 10 Mpc/h sphere around each cluster. The resulting planes are not always aligned: the all filament plane and all halo mass plane are most likely to be aligned, and the largest disagreement between planes for any cluster is most likely to be between the connected filament plane and another plane. The long axis of the cluster tends to lie in the plane as well. Often a perpendicular filament is also present relative to the plane, with others also partially extending out of the sheet. The rough cartoon of the filament shape around clusters is a planar structure with a few filaments sticking out, with a tendency for at least one filament to be close to the plane’s normal direction.

## 5 CORRELATED MASS SCATTER WITH LOCAL FILAMENTARY PLANES

There are observable consequences of the filaments surrounding galaxy clusters: most cluster observations, aside from X-ray<sup>9</sup>, will tend to include some of the cluster environment as well as the cluster itself. We saw above that the majority of the clusters have a preferred direction in their local (10 Mpc/h radius) environments, with a large fraction of their surrounding (connected or all filamentary, or total halo) mass or richness lying in a 3 Mpc/h sheet. The relation of this local structure to observables can be studied by using the mock observations described in WCS. In that work, cluster masses were measured along 96 lines of sight, using six methods mentioned earlier: two richnesses, Compton decrement, weak lensing, and two velocity dispersions. For individual clusters, WCS found correlated outliers in the mass-observable relation along different lines of sight. (It should be noted that Compton decrement and weak lensing both can have significant contamination from beyond the 250 Mpc/h path measured within the box, so correlation with the local environment is likely smaller than found in WCS and below.) Some connection with environment or intrinsic properties is seen: for the 8% of cases where at least two observables had a large ( $\geq 50\%$ ) deviation in mass from that predicted by the mean relation, an excess of nearby galaxies from massive or less massive halos and/or substructure (as detected by the Dressler-Shectman (Dressler & Shectman 1988) test) were found relative to the population without these outliers.

The filamentary structures and mass planes, and the mass fraction in them, provide an additional characterization of individual cluster environments. The WCS mock observations along the 96 lines of sight of each cluster can now be compared to  $|\cos \theta|$ , where  $\theta$  is the angle between the line of sight and the normal to these planes. In addition to the normal to four of the planes mentioned above (connected filament mass, filamentary mass, halo mass, and galaxy richness above  $0.2L_*$ ), we also consider a fifth preferred direction, the angle to the nearest filament, and in this case use  $|\sin \theta_{\text{fil}}|$  of this angle (i.e.  $|\cos \theta|$  of the associated normal to the nearest filament).

The rough expectation is that a cluster’s measured mass along the sheet with the most filamentary mass or total halo

<sup>9</sup> X-ray structure might have some correlation as well, inasmuch as X-ray substructure is related to filaments which provide the cluster’s infalling material.

mass ( $|\cos \theta| \sim 0$ ) will be larger than that along the plane's normal vector. This correlation is not expected to be perfect, as there is often a filament close to the normal, and the fraction and distribution of mass in the plane can vary. In particular, the planes aren't necessarily completely filled, and some directions through this plane might not intersect large amounts of mass (i.e. there might be a lack of isotropy in the plane as mentioned earlier). For planes which are not isotropically filled, one might thus expect a triangular distribution of mass prediction (on the x-axis) vs.  $|\cos \theta|$  (on the y-axis): with low mass values for all  $|\cos \theta|$ , and high mass values for small  $|\cos \theta|$  (along the plane). In addition, planes were defined only within 10 Mpc/h of the cluster, or less, and interlopers are expected to have an effect sometimes at 10 times or more of that distance. These factors suggest that the alignment of an observational direction with a sheet may not be highly noticeable in observations, even if most of the local (filamentary and/or halo) mass lies within this sheet.

Even with these contraindications, for many clusters we found a strong correlation for many mass measures with the angle between the line of sight and the locally defined planes. These strong correlations are seen not only for both measures of richness, which in principle are closely localized to the cluster, but also for weak lensing, and to a lesser extent, SZ. Correlations are both less frequent and less strong for velocity dispersions. We show an example of one cluster's mass scatter for the six observables in Fig. 6. The measured mass is calculated using scaling from the mean mass-observable relation for clusters in the simulation with  $M \geq 10^{14} h^{-1} M_{\odot}$ , and its value is shown versus  $|\cos \theta|$ , where  $\theta$  is the angle between the observational direction and the connected filament plane's normal. The six panels show two richnesses, SZ, weak lensing, and two velocity dispersions. This  $2.7 \times 10^{14} h^{-1} M_{\odot}$  cluster, with 9 filaments, exhibits strong correlations for all six measurements. It has 84% of its connected filament mass and 72% of its halo mass in the connected filament plane.

Given the noisiness of the data, we are mostly interested in general qualitative trends for the full set of 226 cluster nodes. We estimate correlations for each cluster in two ways. One is to use the correlation coefficient for  $(\log M, |\cos \theta|)$ , or the truncated set of points by the procedure described below, if that gives a lower absolute value (i.e. weaker value) for the correlation coefficient. These are shown for our example in Fig. 6 above. By eye, a correlation of  $< -0.25$  appears to be a strong correlation, between  $-0.25$  and  $0.25$  is often (not always) extremely noisy, and a correlation  $> 0.25$  indicates an (unexpectedly) positive correlation. We use this division hereon. A positive correlation is unexpected as this means that measured cluster mass increases as the line of sight intersects less of the preferred plane.

The distributions of these correlation coefficients, for the respective mass measurements in Fig. 6 and the connected filament plane, are shown in Fig. 7 for all 226 cluster nodes. Also printed are the number of clusters with strong (negative), noisy and positive correlations for each measurement. The results are similar for all 5 choices of plane within the considerable noise.<sup>10</sup> The fraction of clusters having

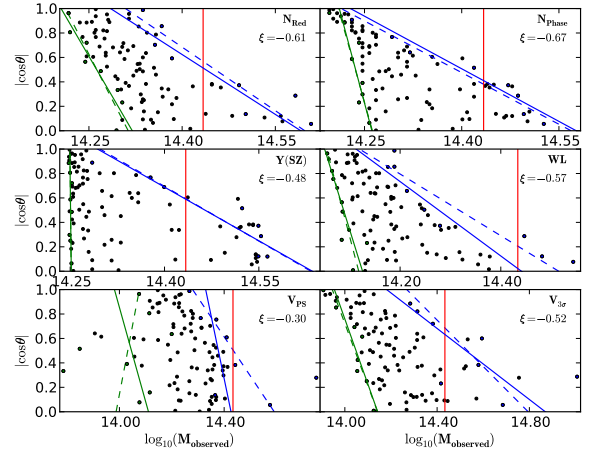


**Figure 6.** Example of mass scatter correlations: each point is a mass measurement for the same cluster along one of  $\sim 96$  lines of sight, having angle  $\theta$  with the normal of the connected filament plane. The vertical line gives the true mass. The mass measurements are based upon (left to right, top to bottom): red galaxy richness, richness based on phase space, Compton decrement, weak lensing, phase based velocity dispersions and  $3\sigma$  clipping velocity dispersions. The mass axes for each measurement vary to cover the range of masses found for that technique, note the scales differ. Envelopes are fit to truncated sets of these points, both using a chi-squared fitting (dashed line) and a shortest perpendicular distance to the envelope (solid line), as described in the text. Where the two severely disagree (e.g. lower left hand box), one or both fits are bad. The correlation coefficients between  $|\cos \theta|$  and  $\log_{10} M/h$  are shown at upper right, they are the smallest in absolute value of those for all or truncated points., or the truncated points. The cluster has mass  $2.7 \times 10^{14} M_{\odot}/h$ , 9 filaments, and about 84% of its connected filament mass in the connected filament plane.

strong negative or positive correlations, split according to type of mass measurement, is shown in table 1, with ranges shown for the 5 choices of plane. The composite correlation of  $\log M_{\text{true}} - \log M_{\text{pred}}$  for all the clusters with  $|\cos \theta|$  followed similar trends, with a strongest correlation coefficient for both richnesses, then weak lensing; velocity dispersions and SZ are all similarly low. The amount of correlation between line of sight and normal to various planes is correlated to some extent with the fraction of mass or richness in these planes, as might be expected. There is also a correlation between the strength of correlations of  $(\log M, |\cos \theta|)$  and the alignments between planes for each cluster (not surprisingly, this depends upon the pair of planes being considered and the plane used to defined  $\theta$ ). Considering multiwave-

then nearest filament (which is lower), there are more strong correlations for weak lensing and Compton decrement, and similar numbers for velocity dispersions. The plane perpendicular to the nearest filament has fewer negative correlations for weak lensing and Compton decrement and many fewer for velocity dispersions. For all 6 mass measurements, the median correlation for the plane perpendicular to the nearest filament is weaker (i.e. more positive) than for the other four planes, by more than the scatter between the median correlations for other four.

<sup>10</sup> Relative to the connected filament plane shown, all other planes have more strong negative correlations for the two richness based masses; for planes besides the plane perpendicular to

property	red richness	phase rich	SZ	weak lensing	phase v	$3\sigma$ v
corrln $< -0.25$	70-80%	85-90%	35-50%	55-75%	20-40%	25-40%
corrln $< -0.25$ or neg rh slope	75-85%	85-95%	40-55%	65-75%	25-40%	30-40%
inertia corrln $< -0.25$	80-85%	75-80%	40-50%	$>90\%$	35-45%	55%
corrln $> 0.25$	$\leq 3\%$	$\leq 3\%$	$\leq 2\%$	1-6%	1-5%	2-7%
corrln $> 0.25$ or large rh pos slope	1 – 4%	2 – 5%	$\leq 3\%$	4-10%	4-9%	2-7%
ill defined slopes	5%	$\sim 0$	$\sim 0$	$\sim 0$	45-50%	50-60%

**Table 1.** Cluster fractions with strongly negative (expected, rounded to the nearest 5%) and positive (unexpected, not rounded) correlation coefficients between  $|\cos \theta|$  and measured mass, by observable, for filament planes, and effect of also considering the inverse slope of the right hand (“rh”) envelopes of the  $(\log M, |\cos \theta|)$  relation, when either strongly negative (expected) or positive (unexpected). and for directions associated with cluster inertia tensor. The range of values encompass those for planes defined with connected filament mass, all filamentary mass within 10 Mpc/h sphere, all halo mass within 10 Mpc/h sphere, galaxy richness, and the plane whose normal is perpendicular to nearest filament to line of sight. Also shown for planes are fractions of clusters with badly defined envelopes (“ill-defined slopes”—suggesting no correlation). The range for strongly negative correlations with two directions of the inertia tensor of the cluster itself (long axis of cluster, using  $\sin \theta$ , or direction of eigenvector with largest eigenvalue) is also shown, see below in text.

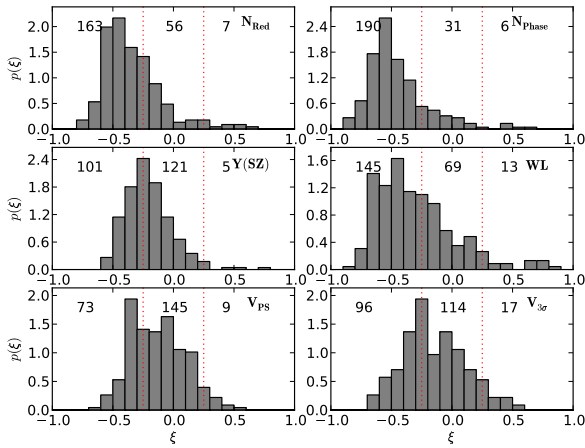


**Figure 7.** Distributions of correlations between measured mass and  $|\cos \theta|$  for the 226 cluster nodes, for six observables. Here  $\theta$  is the angle between the line of sight and the normal to the connected filament plane. The correlation for each cluster is taken to be the one which is minimum in absolute value for all points or the truncated (as described in the text) set of points. The mass measurement methods are as in Fig. 6, i.e., left, right, top to bottom are red galaxy richness, phase space richness, Compton decrement, weak lensing, velocity dispersion using spatial information and  $3\sigma$  clipping velocity dispersion. Also printed for each method are (left) the number of clusters with correlation  $< -0.25$ , (middle) the number of clusters where the correlation’s absolute value is less than 0.25 (and thus possibly noise), and (right) the number of clusters where the correlation is  $> 0.25$ , i.e. both positive and large, indicating a higher mass estimate as the line of sight becomes more perpendicular to the maximal plane. The dashed vertical lines separate these three regions.

length measurements together for each cluster,  $\sim 40$ -50% of the clusters have a strong negative correlation (i.e. the expected sign) for at least 3 observables.

For the planes, the correlation coefficient sometimes

is low, even with a visible trend of measured mass versus  $|\cos \theta|$ . One apparent cause is the expected triangular envelope for the points described above. To identify this pattern, we considered slopes of approximate envelopes of the distributions, shown in Fig. 6. Points are binned in 8 approximately equally filled<sup>11</sup>  $|\cos \theta|$  bins, in each bin  $\leq 2$  points are discarded at large or small  $\log M$  if separated from their nearest neighbor by more than 6 times the median separation in mass in that bin (or the minimum separation if the median is zero). This threw out many of the notable outliers. It also sometimes threw out other points, in a binning dependent way, but the number these points is small and not a concern as we are interested in average overall properties. Points within  $3\sigma$  of the median  $\log M$  are then kept within each  $|\cos \theta|$  bin. Straight line envelopes were then fit to both ends of each bin, either by minimizing perpendicular distance to the envelope or minimizing the chi-squared (note of  $\log M(|\cos \theta|)$ ). Envelopes for both methods are shown in Fig. 6, the cases shown where they strongly disagree correspond to one or both envelopes having bad fits. From hereon we restrict to envelopes based upon minimizing the perpendicular distance to the envelope. The resulting right and left hand inverse slopes are correlated with the correlation coefficients of  $(\log M, |\cos \theta|)$ . We explored adding clusters to the negative (or positive) slope sample which have inverse slopes less than (or more than) the mean value of inverse slope for our correlation coefficient cutoff  $\pm 0.25$ ; the small effect can be seen in table 1. (Sometimes the mean value had the wrong sign, e.g. for velocity dispersions for some choice of plane, which have large scatter, in this case the cutoff was set to zero.) We strove to be conservative in claiming a correlation, so that our estimates for the strength of these planar orientational effects tend to be lower bounds.

Most of the time the envelopes found by our algorithm are reasonable to the eye, but sometimes they fail catastrophically, and were caught by the goodness of fit estimator.

<sup>11</sup> As mentioned earlier, lines of sight where a more massive cluster is present within  $r_{180b}$  are discarded.

The catastrophic failures seem to occur when no correlation is apparent between  $|\cos \theta|$  and measured mass, as does an envelope close to vertical (inverse slope close to zero). The goodness of fits are the worst for the velocity dispersions, which have close to half of the clusters not allowing good fits for either the left or right envelopes, even when the goodness of fit passes threshold, the envelopes are often close to vertical: i.e. the minimum or maximum velocity dispersion mass is similar either perpendicular to the maximum plane or looking through it.

For the unexpected positive correlations, a positive inverse left envelope slope can be understood by looking down a filament near the perpendicular to the plane (small angle, large mass) and then catching a “gap” in the plane (large angle, small mass). It is more difficult to understand  $> 0.25$  correlations or large positive right envelope inverse slopes (i.e. the largest measured mass closer to the perpendicular to the dominant plane). These do not dominate but are not uncommon: for any choice of plane,  $\sim 10\text{--}20\%$  of the clusters have at least one observable with strongly positive inverse right hand slope or correlation (almost half of these are due to velocity dispersions). This dropped to  $< 5\%$  (down to  $1\%$  using the plane perpendicular to the nearest filament or richness) when requiring clusters to have at least 3 observables with either right hand positive slope or correlation (most often weak lensing and both dispersion measurements).

Restricting to correlations, which are a cleaner and more conservative measurement, there are 45 clusters with a positive correlation for at least one measurement (usually velocity dispersions). These clusters differ from the full sample in having, twice as often as the latter, high fractions of perpendicular mass to the connected filament plane and/or some pair of planes misaligned by 60 degrees or a recent merger (as defined earlier). They also slightly more often have another massive cluster within 10 Mpc/h, low mass or richness fraction in some plane, or are more flat (as measured by its inertia tensor, smallest axis/middle axis  $< 0.6$ ). Fewer than a quarter of the clusters with a positive correlation for at least one measurement don’t have one of these factors present, and some of these are close to our cutoffs, e.g. have more mass within 6 Mpc/h (rather than 3 Mpc/h) to the perpendicular to the connected filament plane than most clusters, or planes mismatching by almost 60 degrees. The “unexplained” strongly positive correlations occur for weak lensing and velocity dispersion mass measurements.<sup>12</sup> Given the complexity of the cosmic web, and the small region we use to characterize the cluster’s environment, it is to be expected that our simple cartoon description will not always correlate precisely with observables.

Similar correlations can be calculated using two axes defined from the inertia tensor for the cluster itself: the “long” axis of the cluster, and the normal to the direction of the eigenvector for the largest eigenvalue of its inertia tensor

<sup>12</sup> The fewest cases of strongly positive inverse slope or correlation occur for the plane defined using the perpendicular to the nearest filament to line of sight, suggesting that filaments close to the line of sight might be the cause of positive correlations, but again positive correlations did not always occur for these configurations. However, the plane perpendicular to the nearest filament also gives the fewest (except for richness) strongly negative correlations, i.e. its correlations are weaker in general.

(pointing orthogonal to the longest and middle axes of the cluster). As mentioned earlier, these directions are correlated with the planes, with the “long” cluster axis tending to lie within them and the latter direction tending to align with the plane normals. Compared to the five planes above, the median correlation with mass scatter is stronger for red galaxy richness, weak lensing and the two velocity dispersions, is similar for SZ, and brackets that for phase richness (the long axis of the cluster always has the stronger correlation of the two). The strength of effect for the “long” axis of the cluster is likely due to not only a *plane* being compared to the line of sight, but a specific high density axis within that plane; almost 90% of the clusters have a strong negative correlation for at least 3 of the 6 observables. The fractions of strong negative correlations for these two directions determined by the cluster inertia tensor is also shown in table 1.

In summary, the mass scatter for richness, Compton decrement, weak lensing and velocity dispersion measures is often correlated with the angle to these planes (most for richnesses, and least for velocity dispersions). The correlations aren’t perfect and can sometimes be weak, or even of the opposite sign than expected. In the latter case it is often also true that the different dominant planes (mass, connected or all filamentary halos, and richness) are not well aligned, or that a large filament extends perpendicular to the connected filament plane. Besides being correlated with each other, the planes and the mass scatters are also correlated with axes of the cluster’s inertia tensor.

## 6 CONCLUSION

After implementing a filament finder on an N-body simulation, we studied the resulting filamentary environment for the 226 nodes which are also clusters ( $M \geq 10^{14} M_{\odot}/h$ ). Filaments tend to lie in sheets, presumably those from which they condensed, providing a highly anisotropic environment for the cluster at their center. Within a 10 Mpc/h sphere, we identified sheets of width 3 Mpc/h, centered on each cluster, which maximize either total mass, connected filament mass, all filamentary mass, or galaxy richness. The all filament and halo mass planes are most often closely aligned, while the connected filament plane tends to be within the pair of least aligned planes for the majority of clusters. The direction of the filamentary and mass planes persist slightly as the 10 Mpc/h spheres are extended to 20 Mpc/h. We measured the correlation of mass measurement scatters with the direction of observation relative to these planes for mock observations of richness, Compton decrement, weak lensing and velocity dispersions, via correlation coefficients and fits to the envelopes of the measurements. Often there is a strong correlation between measured mass and direction to the local plane, in spite of the relatively small region (10 Mpc/h radius) used to define the plane (again, this correlation might be overestimated for Compton decrement and weak lensing, which both can have strong scatter from distances larger than our box size). Strong correlations are least likely for velocity dispersions, and fitting envelopes to their distribution of  $|\cos \theta|$  versus  $\log M$  tend to fail badly. This is perhaps not surprising because our finder doesn’t include dynamical information. Alignments of observational direction with two

of the axes of the inertia tensor of the cluster also results in strong correlations with measured mass scatter.

How these planes and correlations with scatter extends to higher redshift depends upon how the finder extends to higher redshift. This is a subtle question as the finder of Zhang et al. (2009) has a built-in scale: a cutoff for minimum halo mass. A full analysis of appropriate generalizations is beyond the scope of this paper; two natural possibilities, however, are to leave the minimum mass alone, or to choose a minimum mass so that the ratio of the number of halos to the number of clusters (107 at  $z = 0.5$ , 25 at  $z = 1.0$ ) remains the same, which gives a minimum mass of  $8.2 \times 10^{10} h^{-1} M_{\odot}$  for  $z = 0.5$  and  $3.0 \times 10^{11} h^{-1} M_{\odot}$  for  $z = 1.0$ .<sup>13</sup> Choosing the latter case (and luminosity cut at  $0.2L^*$ ), most of the trends persist to these higher redshifts, although the total number of filaments in the box decreases. For  $z = 0.5$  and  $z = 1.0$ , the planar mass fractions around clusters are close to unchanged. For all 3 redshifts, there is a slight drop in richness fraction in the richness plane as redshift increases, and the halo mass fraction in planes around random points appears to grow, so that by  $z = 1.0$  it is comparable to that around the 25 clusters in the box at  $z = 1.0$ . For correlations of plane directions with cluster observations, the statistics are very noisy for  $z = 1.0$ , but for  $z = 0.5$ , the fractions of clusters with strong (expected) negative correlations of angle with plane and mass scatter<sup>14</sup>, as in table 1, tend to either remain the same in range or slightly increase (velocity dispersions do decrease in one case), the number of clusters with at least three negative correlations are close to unchanged for three planes, dropping for the richness and nearest filament planes, and positive correlation fractions are about the same except for (an increase for) velocity dispersions. Large plane misalignments are less common, but clusters with misaligned planes still are more likely to have smaller mass fractions in the plane or more perpendicular mass than the full sample.

It would be interesting to determine whether this generalization to higher redshift is appropriate and then to understand the results in terms of the evolution of the filamentary neighborhood of the clusters and the clusters within them.

The correlations between mass scatter and angle of observation with the planes (and inertia tensor of the cluster) rely upon three dimensional information available to us as simulators. It would be very interesting to find a way to make this source of mass bias more evident to observers, perhaps by using a filament finder based upon galaxies directly (amongst those mentioned earlier), and seeing how well they trace these planes, or by combining multiwavelength measurements. In depth studies underway of cluster environments such as Lubin et al. (2009) would be excellent datasets to apply and refine such methods.

We thank Y. Birnboim, O. Hahn, S. Ho, G. Jungman, D. Keres, L. Lubin, S. Nagel, S. Shandarin, A. Szalay, D. Zaritsky and especially M. White for helpful discussions, and we thank M. George, L. Lubin and E. Rozo for helpful comments on the draft. JDC thanks R. Sheth for an introduction to research on filaments, and the Aspen Cen-

ter for Physics for providing the place and opportunity for us to meet and discuss. YN thanks the Santa Fe Cosmology School for the opportunity to present this work, and we both thank the participants there for many useful comments and questions, and S. Habib and K. Heitmann for support in order to be able to attend. Martin White's simulations, used in this paper, were performed at the National Energy Research Scientific Computing Center and the Laboratory Research Computing project at Lawrence Berkeley National Laboratory.

## REFERENCES

- Abell G.O., 1958, ApJS, 3, 211
- Altay, G., Colberg, J. M., & Croft, R. A. C. 2006, MNRAS, 370, 1422
- Aragón-Calvo, M. A., Jones, B. J. T., van de Weygaert, R., & van der Hulst, J. M., 2007a, A & A, 474, 315
- Aragón-Calvo, M. A., van de Weygaert, R., Jones, B. J. T., & van der Hulst, J. M., 2007b, ApJL, 655, L5
- Aragón-Calvo, M.A., Shandarin, S.F., Szalay, A., 2010, arXiv:1006.4178
- Aragón-Calvo, M.A., van de Weygaert, R., Jones, B.J.T., 2010, arXiv:1007.0742
- Bailin, J., & Steinmetz, M., 2005, ApJ, 627, 647
- Barrow, J. D., Bhavsar, S. P., & Sonoda, D. H., 1985, MNRAS, 216, 17
- Basilakos, S.; Plionis, M.; Yepes, G.; Gottlber, S.; Turchaninov, V., 2006, MNRAS, 365, 539
- Becker, M.R., Kravtsov, A.V., 2010, arXiv:1011.1681
- Betancort-Rijo, J.E., Trujillo, I., 2009, arXiv:0912.1051
- Bharadway, S., Sahni, V., Sathyaprakash, B.S., Shandarin, S.F., 2000, ApJ 528, 21
- Biviano, A., Murante, G., Borgani, S., Diaferio, A., Dolag, K., Girardi, M., 2006, A & A, 456, 23
- Bond, N., Strauss, M., Cen, R., 2009, arXiv:0903.3601
- Bond, N.A., Strauss, M.A., Cen, R., 2010, arXiv:1003.3237
- Bond J. R., Kofman L., Pogosyan D., 1996, Nature, 380, 603
- Cen R., 1997, ApJ, 485, 39
- Chambers, S.W., Melott, A.L., Miller, C.J., 2000, ApJ, 544, 104
- Choi, E., Bond, N.A., Strauss, M.A., Coil, A.L., Davis, M., Willmer, C.N.A., 2010, MNRAS, 406, 320
- Colberg, J., White, S.D.M., Jenkins, A., Pearce, F.R., 1999, MNRAS, 308, 593
- Colberg, J., Krughoff, K.S., Connolly, A.J., 2005, MNRAS, 359, 272
- Colberg, J. M., 2007, MNRAS, 375, 337
- Colombi, S., Pogosyan, D., Souradeep, T., 2000, PRL 85, 5515
- Conroy C., Gunn J.E., White M., 2009, ApJ, 699, 486
- Conroy C., White M., Gunn J.E., 2010, ApJ, 708, 58
- Conroy C., Gunn J.E., 2010, ApJ, 712, 833
- Costa-Duarte, M.V., Sodre Jr., L., Durret, F., 2010, arXiv:1010.0981
- Dalton, G.B., Efstathiou, G., Maddox, S.J., & Sutherland, W.J., 1992, ApJL 390, L1
- Davis M., Efstathiou G., Frenk C.S., White S.D.M., 1985, ApJ, 292, 371
- Dekel, A., et al., 2009, Nature, 457, 451

<sup>13</sup> We thank M. White for this suggestion.

<sup>14</sup> The model for color assignments is valid only for  $z = 0.1$ , so we did not consider red galaxy richness at other  $z$ .

- den Hartog, R., Katgert, P., 1996, MNRAS, 279, 349
- Diaferio, A., Geller, M.J., 1997, ApJ, 481, 633
- Diemand J., Kuhlen M., Madau P., 2006, ApJ, 649, 1
- Dolag, K., Meneghetti, M., Moscardini, L., Rasia, E., & Bonaldi, A., 2006, MNRAS, 370, 656
- Dressler A., Sackett S.A., 1988, AJ, 95, 985
- Einasto, J., Klypin, A.A., Saar, E., Shandarin, S.F., 1984, MNRAS, 206, 529
- Faltenbacher, A., Gottlöber, S., Kerscher, M., Muller, V., 2002, A & A, 395, 1
- Faltenbacher, A., Allgood, B., Gottlöber, S., Yepes, G., & Hoffman, Y., 2005, MNRAS, 362, 1099
- Faltenbacher, A., Li, C., Mao, S., van den Bosch, F.C., Yang, X., Jing, Y.P., Pasquali, A., Mo, H.J., 2007, ApJL, 662, 71
- Feix, M., Xu, D., Shan, H., Famaey, B., Limousin, M., Zhao, H., & Taylor, A., 2008, ApJ, 682, 711
- Forero-Romero J.E., Hoffman Y., Gottlöber S., Klypin, A., Yepes G., 2009, MNRAS, 396, 1815
- Gal, R.R., Lemaux, B.C., Lubin, L.M., Kocevski, D., Squires, G.K., 2008, ApJ, 684, 933
- Gay, C., Pichon, C., Le Borgne, D., Teyssier, R., Sousbie, T., & Devriendt, J., 2009, arXiv:0910.1728
- Genovese, C.R., Perone-Pacifico, M., Verdinelli, I., Wasserman, L., 2010, arXiv:1003.5536
- Gonzalez, R.E., Padilla, N., 2009, arXiv:0912.0006, MNRAS to appear
- Hahn, O., Porciani, C., Carollo, C. M., Dekel, A., 2007a, MNRAS, 375, 489
- Hahn, O., Carollo, C. M., Porciani, C., Dekel, A., 2007b, MNRAS, 381, 4
- Hahn, O., Teyssier, R., Carollo, C.M., 2010, arXiv:1002.1964, MNRAS to appear
- Hallman, E.J., O'Shea, B.W., Burns, J.O., Norman, M.L., Harkness, R., Wagner, R., 2007, ApJ 671, 27
- Hoekstra H., 2001, A&A, 370, 743
- Holder, G.P., McCarthy, I.G., Babul, A., 2007, MNRAS 382, 1697
- Hopkins, P.F., Bahcall, N., Bode, N., 2004, ApJ 618, 1
- Jing, Y.P., Suto, Y., 2002, ApJ, 574, 538
- Jones, B.J.T., van de Weygaert, R., Aragón-Calvo, M.A., arXiv:1001.4479
- Kartaltepe, J. S., Ebeling, H., Ma, C. J., & Donovan, D., 2008, MNRAS, 389, 1240
- Kasun S.F., Evrard A.E., 2005, ApJ, 629, 781
- Kereš, D., Katz, Weinberg, D. H. & Davé, R., 2005, MNRAS, 363, 2
- Kereš, D., Katz, N., Fardal, M., Davé, R., & Weinberg, D. H., 2009, MNRAS, 395, 160
- Koester B.P., et al., 2007, ApJ, 660, 221
- Lee, J., 2004, ApJL, 614, L1
- Lee, J., 2006, astro-ph/0605697
- Lee, J., Evrard, A.E., 2007, ApJ 657, 30
- Lee, J., Springel, V., Pen, U.-L., Lemson, G., 2008, MNRAS 389, 1266
- Lee, J., Springel, V., 2009, arXiv:0911.4755, JCAP to appear
- Lubin, L.M., Gal, R.R., Lemaux, B.C., Kocevski, D.D., Squires, G.K., 2009, AJ, 137, 4867
- Lumsden, S.L., Nichol, R.C., Collins, C.A., Guzzo, L., 1992, MNRAS 258, 1
- Mead, J. M. G., King, L. J., & McCarthy, I. G., 2010, MNRAS, 401, 2257
- Mecke, K. R., Buchert, T., & Wagner, H., 1994, A & A, 288, 697
- Meneghetti, M., Fedeli, C., Pace, F., Gottloeber, S., Yepes, G., 2010, arXiv:1003.4544
- Metzler C., White M., Loken C., 2001, ApJ, 547, 560
- Murphy, D.N.A., Eke, V.R., Frenk, C.S., 2010, arXiv:1010.2202
- Novikov, D., Colombi, S., & Doré, O., 2006, MNRAS, 366, 1201
- Onuora, L.I., Thomas, P.A., 2000, MNRAS, 319, 614
- Pandey, B., Somnath, B., 2006, MNRAS, 372, 827
- Paz, D. J., Stasyszyn, F., & Padilla, N. D., 2008, MNRAS, 389, 1127
- Pereira, M. J., Bryan, G. L., & Gill, S. P. D., 2008, ApJ, 672, 825
- Pimbblet, K. A., 2005a, MNRAS, 358, 256
- Pimbblet, K. A., 2005b, Publications of the Astronomical Society of Australia, 22, 136
- Pimbblet, K. A., Drinkwater, M. J., & Hawkrigg, M. C., 2004, MNRAS, 354, L61
- Poggianti, B.M., De Lucia, G., Varela, J., Aragón-Salamanca, A., Finn, R., Desai, V., von der Linden, A., White, S.D.M., 2010, arXiv:1002.3465
- Pogosyan, D., Pichon, C., Gay, C., Prunet, S., Cardoso, J. F., Sousbie, T., & Colombi, S., 2009, MNRAS, 396, 635
- Porter, S. C., & Raychaudhury, S., 2005, MNRAS, 364, 1387
- de Putter R., White M., 2005, New Astronomy, 10, 676
- Ragone-Figueroa, Cinthia; Plionis, Manolis, 2007, MNRAS, 377, 1785
- Reblinsky K., Bartelmann M., 1999, A&A, 345, 1
- Sahni, V., Sathyaprakash, B. S., & Shandarin, S. F., 1998, ApJL, 495, L5
- Schäfer, B. M., 2009, International Journal of Modern Physics D, 18, 173
- Schmalzing, J., , 1998, Proceedings of the 12th Potsdam Cosmology Workshop (1997). Eds. V.Mueller, S.Gottloeber, J.P.Muecket, J.Wambsganss, 195ff
- Schmalzing, J., Buchert, T., Melott, A. L., Sahni, V., Sathyaprakash, B. S., & Shandarin, S. F., 1999, ApJ, 526, 568
- Shandarin, S.F., Zel'dovich, Ia. B., 1983, Comments on Astrophysics, 10, 33
- Shandarin, S.F., 2004, astro-ph/0405303
- Shandarin, S.F., Sheth, J.V., Sahni, V., 2004, MNRAS, 353, 162
- Shandarin, S. F., Habib, S., Heitmann, K., 2009, arXiv:0912.4471
- Shandarin, S., 2010, arXiv:1011.1924
- Shaw, L.D., Holder, G.P., Bode, P., 2008, ApJ, 686, 206
- Shen, J., Abel, T., Mo, H. J., & Sheth, R. K., 2006, ApJ, 645, 783
- Sheth, J.V., Sahni, V., Shandarin, S.F. & Sathyaprakash, B., 2003, MNRAS, 343, 22
- De Simone, A., Maggiore, M., Riotto, A., 2010, arXiv:1007.1903
- Skibba, R. A., Sheth, R.K., 2009, MNRAS 392, 1080
- Song, H, Lee, J., 2010, arXiv:1006.4101
- Sousbie, T., Pichon, C., Courtois, H., Colombi, S., & Novikov, D., 2008a, ApJL, 672, L1

- Sousbie, T., Pichon, C., Colombi, S., Novikov, D., & Pogosyan, D., 2008b, MNRAS, 383, 1655
- Sousbie, T., Colombi, S., & Pichon, C., 2009, MNRAS, 393, 457
- Sousbie, T., 2010, arXiv:1009.4015
- Sousbie, T., Pichon, C., Kawahara, H., 2010, arXiv:1009.4014
- Stoica, R. S., Martínez, V. J., Mateu, J., & Saar, E., 2005, A & A, 434, 423
- Stoica, R. S., Martinez, V. J., & Saar, E., 2008, arXiv:0809.4358
- Stoica, R.S., Martinez, V.J., Saar, E., 2009, arXiv:0912.2021
- Splinter, R.J., Melott, A. L., Linn, A., Buck, C., Tinker, J., 1997, ApJ, 479, 632
- Sunyaev R. A. & Zel'dovich, Ya. B., 1972, 1972, Comm. Astrophys, Space Phy., 4, 173
- Sunyaev R. A. & Zel'dovich, Ya. B., 1980, ARA&A, 18, 537
- Tanaka, M., Finoguenov, A., Kodama, T., Koyama, Y., Maughan, B., & Nakata, F., 2009, A & A, 505, L9
- Tormen G., 1997, MNRAS, 290, 411
- van Haarlem, M., van de Weygaert, R., 1993, ApJ, 418, 544
- van Haarlem M.P., Frenk C.S., White S.D.M, 1997, MNRAS, 287, 817
- van de Weygaert, R., Bertschinger, E., 1996, MNRAS, 281, 84
- van de Weygaert, R., 2002, 2002, Proceedings 2nd Hellenic Cos- mology Workshop, 0, 153ff
- van de Weygaert, R., 2006, arXiv:astro-ph/0607539
- van de Weygaert, R., & Schaap, W., 2007, arXiv:0708.1441
- van de Weygaert, R., Vegter, G., Platen, E., Eldering, B., Kruithof, N., 2010, arXiv:1006.2765
- Voit, G.M., 2005, Rev. Mod. Phys. 77, 207
- Wang, H., Mo, H. J., Jing, Y. P., Guo, Y., van den Bosch, F. C., & Yang, X., 2009, MNRAS, 394, 398
- Wang, H., Mo, H.J., Jing, Y.P., Yang, X., Wang, Y., 2010, arXiv:1007.0612
- Way, M.J., Gazis, P.R., Scargle, J.D., 2010, arXiv:1009.0387
- White, R., et al 1999, AJ 118, 2014
- White M., 2001, A&A, 367, 27
- White, M., Hernquist, L., Springel, V., 2002, ApJ, 579, 16
- White M., 2002, ApJS, 143, 241
- White, M., Cohn, J.D., Smit, R., 2010, arXiv:1005.3022, MNRAS to appear
- Wojtak, R., Lokas, E.L., Mamon, G.A., Gottlober, S., Prada F., Moles M., 2007, A&A 466, 437
- Wray, J.J., Bahcall, N.A., Bode, P., Boettiger, C., Hopkins, P.F., 2006, ApJ 652, 907
- Wu, Y., Batuski, D.J., Khalil, A., 2009, ApJ 707, 1160
- Yang X., Mo H.J., van den Bosch F.C., 2008, ApJ, 676, 248
- Zel'dovich, Ia.B., Einasto, J., Shandarin, S.F., 1982, Nature, 300, 407
- Zhang, Y., Yang, X., Faltenbacher, A., Springel, V., Lin, W., Wang, H., 2009, ApJ, 706, 747